Journal of Membrane Science 618 (2021) 118555

Contents lists available at ScienceDirect

Journal of Membrane Science

journal homepage: http://www.elsevier.com/locate/memsci

Exploring the performance limits of MOF/polymer MMMs for O_2/N_2 separation using computational screening

Hilal Daglar [a], Ilknur Erucar [b], Seda Keskin [a,*]

[a] Department of Chemical and Biological Engineering, Koc University, Rumelifeneri Yolu, Sariyer, 34450, Istanbul, Turkey
[b] Department of Natural and Mathematical Sciences, Faculty of Engineering, Ozyegin University, Cekmekoy, 34794, Istanbul, Turkey

ARTICLE INFO

Keywords:
Metal organic framework
Air separation
Membrane
Molecular simulations
Selectivity

ABSTRACT

Air separation is one of the most challenging separations because of the very similar molecular dimensions of gas molecules. We used a high-throughput computational screening approach to identify the upper performance limits of metal organic framework (MOF) membranes and MOF/polymer mixed matrix membranes (MMMs) for O_2/N_2 separation. Gas permeabilities and selectivities were calculated for 5629 MOF membranes and 78,806 different types of MOF/polymer MMMs, which represent the largest number of MOF-based membranes studied to date for air separation. Our results showed that many MOF membranes exceed the upper bound established for polymer membranes due to their high permeabilities and/or selectivities. The maximum achievable O_2 permeability and O_2/N_2 selectivity of MOF/polymer MMMs were computed as 2710.8 Barrer and 19.8, respectively. Results revealed that MOF/polymer MMMs can outperform MMMs composed of traditional fillers, such as zeolites, in terms of O_2 permeability and O_2/N_2 selectivity. The impacts of purity of air mixture and the structural flexibility of MOFs on the gas separation performances of MMMs were also discussed. These results provide molecular-level insights into adsorption and diffusion behaviors of O_2 and N_2 in MOF membranes in addition to presenting structure-performance relations of MOFs that can lead to high-performance membranes and fillers for MMMs.

1. Introduction

Metal organic frameworks (MOFs) are ideal membrane materials for various gas separations due to their high porosities, large surface areas, and appealing chemical functionalities [1]. One of the challenges in this field is to select the superior MOF membranes offering both high selectivity and high permeability to achieve an effective gas separation. There are almost 100,000 experimental MOFs reported in the Cambridge Structural Database (CSD) [2] according to November 2019 version and it is not practical to fabricate and test each MOF membrane for a target gas separation using purely experimental methods. Molecular simulations, which can accurately compute adsorption and diffusion of gas molecules within the pores of MOFs in a time-efficient manner, are highly useful to predict gas separation performances of MOF membranes prior to experiments. High-throughput computational screening methods employing atomically detailed simulations identify the best performing MOF membranes among several thousands of candidates and direct experiments to those promising materials. Several excellent reviews [3–7] address the importance of using computational screening methods to unlock membrane gas separation performances of MOF membranes.

Almost all large-scale computational studies of MOFs focused on CO_2 separation. For example, Watanabe and Sholl [8] used a multi-step screening approach to identify 10 promising MOFs having membrane selectivities >1000 among 359 MOFs having suitable pore diameters for membrane-based CO_2/N_2 separation. Qiao et al. [9] used 137,953 hypothetical MOFs and examined their membrane-based $CO_2/N_2/CH_4$ separation performances and identified 24 top-performing MOF membranes for the single-step separation of CO_2 and N_2 from CH_4 at infinite dilution. To consider the real operation conditions for upgrading the natural gas, they then screened the computation-ready, experimental (CoRE) MOF database consisting of 4764 MOFs for $CO_2/N_2/CH_4$ mixture at 10 bar and 298 K [10]. Promising MOF membranes having CO_2/CH_4 selectivities of 704–8157 were selected for separation of CO_2 and N_2 from the $CO_2/N_2/CH_4$ mixture. Our group used a high-throughput computational screening approach to study the most recent MOF database and identified the best MOFs for various membrane-based gas separations including H_2/CO_2 [64], CO_2/N_2 [12], and CO_2/CH_4 [13].

* Corresponding author.
E-mail address: skeskin@ku.edu.tr (S. Keskin).

https://doi.org/10.1016/j.memsci.2020.118555
Received 8 June 2020; Received in revised form 23 July 2020; Accepted 27 July 2020
Available online 1 August 2020
0376-7388/© 2020 The Authors. Published by Elsevier B.V. This is an open access article under the CC BY-NC-ND license (http://creativecommons.org/licenses/by-nc-nd/4.0/).

Air separation, mainly O_2/N_2 separation, is important for the carbon capture in an oxy-fuel combustion process [14]. On the other hand, this separation is one of the most challenging ones because the kinetic diameters of O_2 (3.46 Å) and N_2 (3.64 Å) are very close to each other [15]. The majority of the computational studies focused on either O_2 storage or adsorption-based O_2/N_2 separation. For example, 2932 CoRE MOFs were screened to identify the best performing MOFs for O_2 storage and MOFs exhibiting the highest volumetric and gravimetric O_2 working capacities were identified [16]. McIntyre et al. [17] computationally examined the O_2/N_2 separation performance of isoreticular MOFs (IRMOFs) and reported that O_2/N_2 selectivities vary between 1 and 1.3, showing that these MOFs are almost unselective. Demir et al. [18] recently performed molecular simulations of 261 CoRE MOFs for adsorption-based O_2/N_2 separation and showed that among 261 MOFs, 210 MOFs have O_2/N_2 selectivity >1 but the maximum selectivity was reported as 1.4, indicating the difficulty of finding highly selective MOFs for this separation. Several experimental studies have focused on both pure MOF membranes [19–22] and MOF/polymer mixed matrix membranes (MMMs) [23–31] where MOFs as fillers are incorporated into polymers to resolve the trade-off between O_2 permeability and selectivity of polymers [32]. On the other hand, there is only one computational study on predicting O_2/N_2 separation performance of MOF membranes in which membrane selectivities of 44 MOFs were found to be in the range of 1.5–11 [33].

The number of MOFs has been rapidly increasing and we still do not know O_2/N_2 separation performance limits of pure MOF membranes and MOF/polymer MMMs. Herein, we investigated the O_2/N_2 separation potential of MOF membranes using a large-scale computational screening approach. Adsorption and diffusion properties of 5629 MOFs were computed using Grand Canonical Monte Carlo (GCMC) and Molecular Dynamics (MD) simulations at two different conditions. Using this data, O_2/N_2 selectivities and O_2 permeabilities of MOF membranes were calculated and compared with traditional membranes. Structure-performance relations were examined to reveal the desired structural features of MOFs that can lead to highly selective membranes. We then calculated gas permeabilities and selectivities of 78,806 different types of MOF/polymer MMMs composed of 5629 MOFs and 14 polymers, which represents the largest number of MOF/polymer MMMs studied to date for air separation. Our results identified the upper performance limits of MMMs and the top promising MOF/polymer pairs for air separation. The impacts of purity of air mixture on the gas separation performances of MMMs were discussed in detail. Finally, computationally demanding flexible MD simulations were performed to explore the impact of structural flexibility of MOFs on the O_2/N_2 separation performances of MMMs.

2. Computational methods

2.1. MOFs and polymers

The crystallographic information of MOF structures was obtained from the updated CoRE MOF 2019 database consisted of 12,020 solvent-free materials [34]. Zeo++ code (version 0.3) [35] was used to obtain structural features of MOFs including pore limiting diameter (PLD), the largest cavity diameter (LCD), accessible surface area, density, and pore volume. 1.86 Å, which is the kinetic radius of N_2 molecule, was used as the probe size for surface area calculations. Geometric pore volumes were computed using a probe radius of 0 Å and 5×10^4 trials. We excluded the MOFs for which O_2 and N_2 diffusivities were computed to be $<10^{-8}$ cm^2/s, the limit of MD simulations to accurately compute self-diffusivities of gases. Consequently, we ended up with 5629 MOFs with PLDs >3.72 Å to allow the transport of O_2 and N_2 through the pores.

We focused on 14 different polymers, PSF [27], Matrimid [24], PU [30], PPEES [36], BPDA-ODA [37], BTDA-ODA [37], PEI [38], 6FDA/PMDA ((25/75)-TAB) [39], Sulfonated PPO [40], BADBSBF-BTDA [41], PTMSDPA [42], ODPA-TMDPA [43], PIM-1 [44] and PIM-7 [44]. PSF, Matrimid, PU, PPEES, and ODPA-TMA were selected since they are commonly used for separating O_2 from N_2 in the experimental studies. We chose the other polymers based on their closeness to the Robeson's upper bound [32] since the incorporation of MOFs into these polymers may carry them above the upper bound. We note that we considered the 2008 Robeson's upper bound throughout this study. Experimentally measured gas permeabilities and O_2/N_2 selectivities of polymers were taken from the literature and listed in Table S1 of the Supplementary data (SM).

2.2. Molecular simulations

Henry's constants of O_2 and N_2 ($K^0_{O_2}$, $K^0_{N_2}$) and their isosteric heats of adsorption (Q^0_{st}) at infinite dilution were computed by the Widom insertion method at 298 K [45]. 1.5×10^4 MC cycles, with 5×10^3 initialization and 10^4 production cycles, were used to compute $K^0_{O_2}$, $K^0_{N_2}$ values. Equilibrium MD simulations were performed to obtain self-diffusivities of gases ($D^0_{O_2}$, $D^0_{N_2}$) in MOFs at infinite dilution, 298 K. To represent the infinite dilution, adsorbate-adsorbate interactions were not considered in MD simulations, and 30 gas molecules were inserted into the pores of MOF. These simulations were performed at NVT ensemble using a time step of 1 fs and 10^6 cycles. Single-component gas adsorption and diffusion data of MOFs were computed using GCMC and MD simulations at 1 bar and 298 K. We also performed binary (O_2/N_2:20/80) and ternary (O_2/N_2/Ar:20.98/77.92/1.1) mixture simulations for selected MOFs at 298 K and 1 bar. We carried out all molecular simulations using the RASPA software [46]. To consider the effect of structural flexibility of MOFs, flexible MD simulations were carried out with the Materials Studio 2020 (MS) [47] simulation package for only two representative MOFs. As we discussed in our previous work [48], gas adsorption results obtained from RASPA and MS were found to be in agreement. More details of the GCMC and MD simulations were provided in the SM.

2.3. Membrane calculations

We studied two different conditions in molecular simulations to examine the potential of MOF membranes for O_2/N_2 separation: (i) infinite dilution at 298 K, (ii) 1 bar and 298 K. We calculated adsorption, diffusion, and membrane selectivities of 5629 MOFs at these two conditions and compared the results to reveal how the predicted gas separation performances of membranes change based on the simulation conditions. Adsorption selectivity at infinite dilution, $S^0_{ads,N_2/O_2}$, was calculated by using the ratios of $K^0_{N_2}$ *and* $K^0_{O_2}$. Adsorption selectivity at single-component gas condition, $S^{SC}_{ads,N_2/O_2}$, was computed as the ratio of adsorbed gas uptakes $N^{SC}_{N_2}$ *and* $N^{SC}_{O_2}$ obtained from GCMC simulations performed at 1 bar, 298 K. We note that binary (O_2/N_2:20/80) and ternary (O_2/N_2/Ar:20.98/77.92/1.1) mixture adsorption selectivities, $S^{MIX}_{ads,O_2/N_2}$, were calculated only for the top 10 MOFs leading to the highest O_2/N_2 selectivities for MMMs. Mixture selectivity was calculated using the ratio of adsorbed gas amounts obtained from mixture simulations $N^{MIX}_{O_2}$*and* $N^{MIX}_{N_2}$, normalized by the bulk gas composition, $y^{MIX}_{O_2}$*and* $y^{MIX}_{N_2}$, at 1 bar and 298 K as follows:

$$S^0_{ads,N_2/O_2} = K^0_{N_2}/K^0_{O_2},$$
$$S^{SC}_{ads,N_2/O_2} = N^{SC}_{N_2}/N^{SC}_{O_2},$$
$$S^{MIX}_{ads,N_2/O_2} = \left(N^{MIX}_{N_2}/N^{MIX}_{O_2}\right)/\left(y^{MIX}_{N_2}/y^{MIX}_{O_2}\right) \quad (1)$$

The differences of heat of adsorption of gases computed at infinite dilution, ΔQ^0_{st}, and at single-component condition ΔQ^{SC}_{st}, were calculated from the corresponding GCMC simulations:

$$\Delta Q_{st}^{0} = Q_{st,O_2}^{0} - Q_{st,N_2}^{0},\ \Delta Q_{st}^{SC} = Q_{st,O_2}^{SC} - Q_{st,N_2}^{SC} \quad (2)$$

Diffusion selectivity at infinite dilution, $S_{diff,O_2/N_2}^{0}$, was calculated by using the ratios of $D_{O_2}^{0}$ *and* $D_{N_2}^{0}$. Similarly, single-component, binary, and ternary mixture diffusion selectivities were calculated by using the ratios of gas diffusivities at 1 bar as follows:

$$S_{diff,O_2/N_2}^{0} = D_{O_2}^{0}/D_{N_2}^{0},$$
$$S_{diff,O_2/N_2}^{SC} = D_{O_2}^{SC}/D_{N_2}^{SC},$$
$$S_{diff,O_2/N_2}^{MIX} = D_{O_2}^{MIX}/D_{N_2}^{MIX} \quad (3)$$

Gas permeabilities at infinite dilution, P_i^0, were estimated by multiplying K_i^0 with D_i^0. However, gas permeabilities of MOFs for single-component, binary, and ternary mixtures at 1 bar and 298 K were calculated by using the adsorbed gas loadings (c) computed from GCMC simulations, self-diffusion coefficients obtained from MD simulations, and the partial pressure (f) of the gas species (i) as follows:

$$P_i^0 = K_i^0 \times D_i^0,$$
$$P_i^{SC} = c_i^{SC} \times D_i^{SC}/f_i,$$
$$P_i^{MIX} = c_i^{MIX} \times D_i^{MIX}/f_i \quad (4)$$

Finally, membrane selectivities of MOFs were calculated at infinite dilution (S_{mem}^{0}), single-component gas (S_{mem}^{SC}), binary and ternary mixture conditions (S_{mem}^{MIX}) as follows:

$$S_{mem,O_2/N_2}^{0} = P_{O_2}^{0}/P_{N_2}^{0},$$
$$S_{mem,O_2/N_2}^{SC} = P_{O_2}^{SC}/P_{N_2}^{SC},$$
$$S_{mem,O_2/N_2}^{MIX} = P_{O_2}^{MIX}/P_{N_2}^{MIX} \quad (5)$$

In a previous work, we explained the good agreement between experimental and simulated gas permeabilities of various MOF/polymer MMMs using the Maxwell model [49], a permeation model based on ideal morphology approximation [50]. Motivated from this agreement, the Maxwell model was applied to calculate gas permeabilities of MMMs as shown below:

$$P^{MMM} = P^{P} \times \left[\frac{2\times(1-\varphi)+(1+2\varphi)\times\left(P^{MOF}/P^{P}\right)}{(2+\varphi)+(1-\varphi)\times\left(P^{MOF}/P^{P}\right)}\right] \quad (6)$$

Here, P^{MMM} is the gas permeabilities of MMMs, P^{MOF} is the gas permeability of MOF, P^{P} is the gas permeability of polymer that we collected from the experimental literature, and φ is the volume fraction of MOF filler which was used as 0.2 according to the literature on experimentally fabricated MOF/polymer MMMs [49]. Finally, we calculated O_2/N_2 selectivity of MOF/polymer MMMs (S_{O_2/N_2}^{MMM}) as follows:

$$S_{O_2/N_2}^{MMM} = P_{O_2}^{MMM}/P_{N_2}^{MMM} \quad (7)$$

3. Results and discussions

3.1. Separation performance of pure MOF membranes

Large-scale molecular simulations to assess the performance of MOF membranes are generally performed at infinite dilution since gas-gas interactions are ignored in simulations at this condition which significantly shortens the simulation time. However, to ensure the accuracy of simulation results, single-component gas simulations should be performed at predefined operating conditions. Therefore, we performed molecular simulations for adsorption and diffusion of single-component O_2 and N_2 gases at 1 bar and 298 K in addition to infinite dilution. Adsorption, diffusion, and membrane selectivities of MOFs were computed at these two conditions and compared in Fig. 1 to examine the effect of simulation conditions on the predicted separation performances of 5629 MOF membranes.

We first discuss adsorption selectivities of MOFs for air separation.

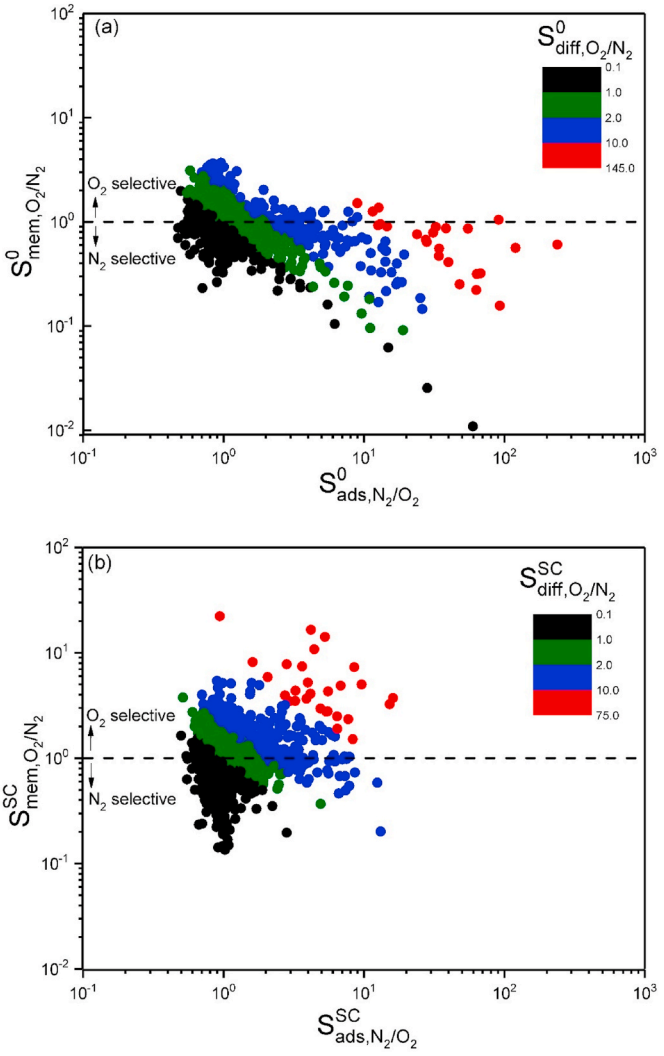


Fig. 1. Adsorption, diffusion, and membrane selectivities of 5629 MOFs for O_2/N_2 separation (a) computed at infinite dilution (b) using the single-component gas data at 1 bar, 298 K.

Since N_2 is generally more strongly adsorbed than O_2 due to its higher quadrupole moment than O_2 [51], adsorption selectivities were reported for N_2 over O_2 in Fig. 1. We also provided Fig. S1 to represent O_2/N_2 adsorption selectivity of MOFs. Calculated average K^0 values for O_2 (~5×10^{-6} mol/kg/Pa) and N_2 (~7×10^{-6} mol/kg/Pa) were found to be similar for most of the MOFs, suggesting that usage of MOFs as adsorbents is not feasible for O_2 separation from N_2. 5386 MOFs exhibited a non-selective behavior because their $S_{ads,N_2/O_2}^{0}$ values were computed to be almost 1. 235 MOFs provided higher K^0 values for N_2 than O_2, indicating that these MOFs can be N_2 selective adsorbents offering $S_{ads,N_2/O_2}^{0}$ values between 2 and 239. Only 8 MOFs exhibited slightly higher K^0 values for O_2 than N_2, resulting in $S_{ads,O_2/N_2}^{0}$ values around 2.

Similar results were found for adsorption selectivities of MOFs calculated from the single-component adsorption data at 1 bar and 298 K. For 5443 MOFs, $S_{ads,N_2/O_2}^{SC}$ values were calculated to be almost unity whereas $S_{ads,N_2/O_2}^{SC}$ values of 182 MOFs ranged from 2 to 16. Only 4 MOFs exhibited higher selectivity towards O_2 with a value of 2. Selectivities calculated from single-component gas simulations ($0.5 \leq S_{ads,N_2/O_2}^{SC} \leq 16.1$) were found to be much lower than those computed at infinite dilution ($0.5 \leq S_{ads,N_2/O_2}^{0} \leq 238.5$) as shown in Fig. S2a. Similarly, CO_2/N_2 selectivities of MOFs computed at infinite dilution were reported to be

higher than the selectivities calculated at 1 bar when MOF-CO_2 affinity was very strong [52]. Strong MOF-N_2 affinity was observed in this work as evidenced by the difference of heat of adsorption values of gases. For example, the heat of adsorption values of MOFs for N_2 were calculated to be between -37.7 and -1.4 kJ/mol at 1 bar, 298 K, whereas they were calculated to be between -44.3 and -1.3 kJ/mol at infinite dilution, 298 K. On the other hand, the heat of adsorption values of O_2 at infinite dilution (between -1.2 and -26.5 kJ/mol) were found to be similar to those at 1 bar, 298 K (between -1.2 and -26.4 kJ/mol), resulting in lower ΔQ_{st}^{SC} values (between -5.1 and 20.9 kJ/mol) than ΔQ_{st}^{0} (between -6.9 and 28.7 kJ/mol) as shown in Fig. S2b. As a result, the higher ΔQ_{st}^{0} values computed infinite dilution led to higher adsorption selectivities at this condition.

Weakly adsorbed O_2 molecules in the majority of MOFs diffuse faster within the pores compared to the strongly adsorbed N_2 molecules. Self-diffusivities of O_2 and N_2 in MOFs at infinite dilution (1 bar) were computed to be between 3.2×10^{-6}– 3.3×10^{-3} cm^2/s (3.2×10^{-6}– 2.4×10^{-3} cm^2/s) and 1.2×10^{-6}– 2.4×10^{-3} cm^2/s (9.5×10^{-7}– 3×10^{-3} cm^2/s), respectively. Colored symbols in Fig. 1 represent the spreading of diffusion selectivities. $S^{0}_{diff,O_2/N_2}$ values range from 0.16 to 144.3 whereas $S^{SC}_{diff,O_2/N_2}$ values range from 0.13 to 74.6. Black symbols in Fig. 1a and b represent 2676 and 2409 MOFs for which N_2 diffusion was faster than O_2 at infinite dilution and 1 bar, respectively. Blue symbols show MOFs having almost the same diffusion selectivities. There are large numbers of MOFs, 2739 MOFs at infinite dilution and 2879 MOFs at 1 bar, exhibiting a non-selective diffusion behavior. Green symbols in Fig. 1 show MOFs having faster O_2 diffusion than N_2, leading to $S_{diff,O_2/N_2}$ values of 2–10 for 191 (313) MOFs at infinite dilution (1 bar). Finally, red symbols represent the MOFs (23 MOFs at infinite dilution and 28 MOFs at 1 bar) showing high diffusion selectivity towards O_2. In these MOFs, O_2 diffusion was found to be at least one order of magnitude higher than N_2 diffusion. Using adsorption and diffusion selectivities, membrane selectivities of MOFs were calculated for O_2/N_2 separation. Membrane selectivities of MOFs at infinite dilution ($S^{0}_{mem,O_2/N_2}$) were computed to be lower, 0.01–3.7, than those computed at single-component condition, 0.13–22.2 ($S^{SC}_{mem,O_2/N_2}$). As expected, the higher number of MOF membranes (269) exhibited O_2 selective behavior at 1 bar than those (158) at infinite dilution. Since O_2/N_2 adsorption selectivities were computed to be almost unity for most of the O_2 selective MOF membranes at infinite dilution and 1 bar, diffusion selectivities determined the membrane selectivities.

We estimated O_2 and N_2 permeabilities of MOFs using single-component gas uptakes and diffusivities because permeation data of polymer membranes have been generally reported for single-component gases in the literature and our aim is to compare MOF membranes with polymers. Fig. 2 shows O_2 permeabilities and O_2/N_2 selectivities of 5629 MOF membranes calculated at 298 K and 1 bar. The Robeson's upper bound established for O_2/N_2 separation was represented with the red line. O_2 permeabilities of MOFs were computed to be between 2.4×10^{3} and 4×10^{6} Barrers, while O_2/N_2 selectivities were calculated as 0.13–22.2. MOFs have higher O_2 permeabilities than polymers (4×10^{-4}–2×10^{4} Barrers) [32], for this reason, we extrapolated the upper bound with a dashed line as shown in Fig. 2. Many MOFs surpass the Robeson's bound owing to their high permeabilities and/or selectivities, indicating that MOF membranes can be strong alternatives to polymers for O_2/N_2 separation. As we discussed above, the biggest challenge in this field is the low membrane selectivity due to similar kinetic diameters of O_2 and N_2. Therefore, identifying MOF membranes having higher selectivity than polymers is important.

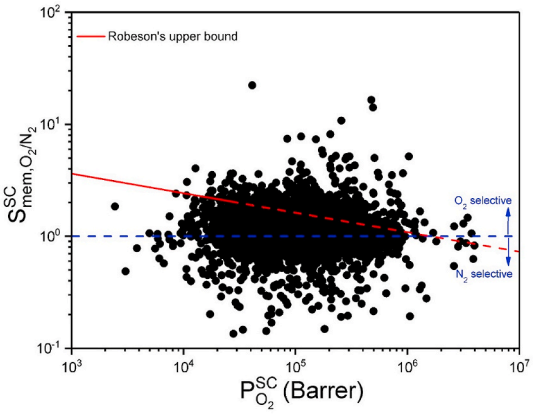


Fig. 2. Computed O_2/N_2 selectivities and O_2 permeabilities of 5629 MOFs. Red line represents the 2008 Robeson's upper bound [32]. (For interpretation of the references to color in this figure legend, the reader is referred to the Web version of this article.)

We identified the top 10 promising MOF membranes that offer high O_2/N_2 selectivities in the range of 5.4–22.2 and high O_2 permeabilities in the range of 4.1×10^{4}– 5×10^{5} Barrer and listed them in Table S3. High diffusion selectivities of MOFs towards O_2 ($S^{SC}_{diff,O_2/N_2}$ ≥5) were responsible for their high membrane selectivities. These MOFs generally have small PLDs (3.74–5.33 Å) and the LCDs (4.85–5.72 Å) except PAJSAX which has large pore dimensions (11.2 × 11.73 Å). Due to this, both N_2 and O_2 uptakes were predicted to be similar and quite low (almost 0.3 mol/kg) at 1 bar, resulting in an adsorption selectivity of almost unity. Faster diffusion of O_2 (6×10^{-5} cm^2/s) in PAJSAX compared to that of N_2 (2.9×10^{-6} cm^2/s) led to a much higher O_2 permeability and made this MOF an O_2 selective membrane. To better understand the effect of structural features of MOFs on their gas separation performances, relations between all selectivity types and structural properties such as the LCDs and porosities are analyzed in Fig. S3. MOFs with small pores generally have high N_2/O_2 adsorption selectivities (Fig. S3a) because narrow pores lead to strong confinement of gas molecules and N_2 is more strongly adsorbed than O_2 within the majority of MOFs. Weakly adsorbed O_2 molecules can diffuse faster than the strongly adsorbed N_2 molecules in the narrow pores, which generally offers high O_2/N_2 diffusion selectivities (Fig. S3b). As a result, MOF membranes with narrow pore sizes (<5 Å) and low porosities (0.2–0.6) generally have high O_2/N_2 separation performances as supported by Fig. S3c. O_2 and N_2 permeabilities were also plotted as a function of PLDs and porosities as shown in Fig. S4. Since permeability is a combination of adsorption and diffusion, we obtained similar trends between gas permeabilities and structural properties (PLDs and porosities) with those obtained between membrane selectivities and structural properties (LCDs and porosities) as given in Fig. S3. Overall, when the porosities and pore sizes of MOFs increase, membranes become non-selective.

3.2. Separation performances of MOF/polymer MMMs

In previous parts, we have discussed the O_2/N_2 separation potential of MOFs as pure membranes. Fabrication of continuous and defect-free porous membranes has been always challenging due to the deficient intergrowth at the interface of membrane-support and reproducibility of the fabrication techniques to obtain membranes with the same separation performance [53]. To tackle these challenges, experimental efforts have been recently shifted from pure MOF membranes to MOF/polymer MMMs, where MOFs have been used as fillers in polymers to enhance their gas separation performances. Polymer membranes are commonly chosen for air separation due to their economical, modular, and scalable design. However, commercial polymers are not capable of producing high purity O_2 since they generally have low O_2 permeability (0.05–370 Barrer) and moderate O_2 selectivity (3.3–10.5) [54]. Before predicting gas permeabilities of large numbers of MOF/polymer MMMs using molecular simulations, we first showed the validity of our computational method by comparing our simulated O_2 and N_2 permeabilities with the experimentally available gas permeability data [26,27,30,36,

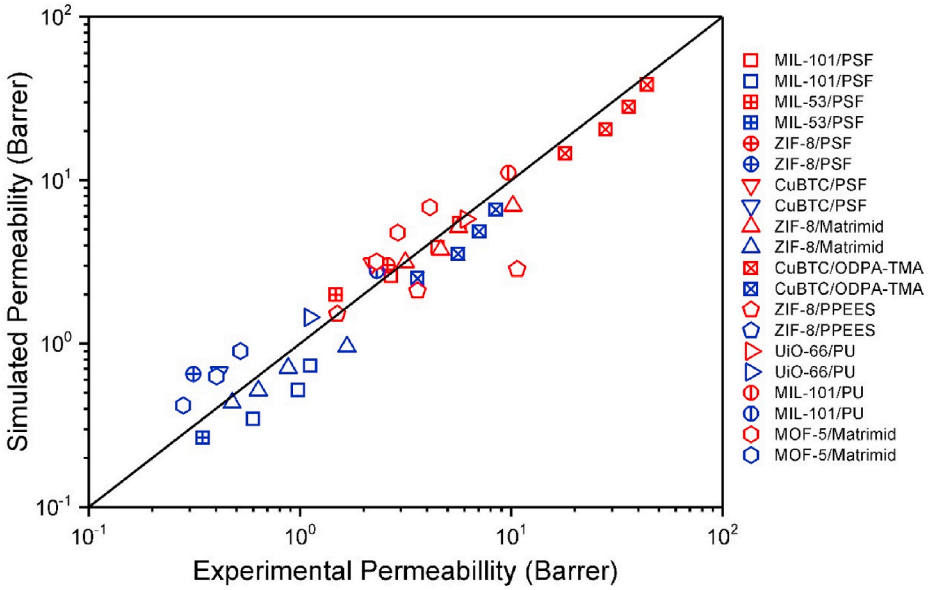


Fig. 3. Comparison of experimental and simulated gas permeabilities of MOF-based MMMs. Red (blue) represents O_2 (N_2) permeabilities of MMMs. (For interpretation of the references to color in this figure legend, the reader is referred to the Web version of this article.)

43,55,56] of different MOF/polymer MMMs. To accurately compare simulation results with experiments, we performed molecular simulations at the same pressures, temperatures and using the same filler volume fractions with the experiments as reported in Table S4. Fig. 3 shows the good agreement between our predictions and experiments for single-component N_2 and O_2 permeabilities of 10 different MMMs composed of well-known MOFs including UiO-66, ZIF-8, Cu-BTC, MOF-5, MIL-53 and MIL-101 and commonly used polymers such as Matrimid, PSF, PPEES, PU, ODPA-TMA. Motivated from this good agreement, we examined 78,806 MOF/polymer MMMs composed of 14 polymers and 5629 MOFs using the Maxwell model.

Fig. 4 shows that O_2/N_2 selectivities and O_2 permeabilities of MOF/polymer MMMs were computed to be between 0.14–2.7×10^3 Barrers and 2.3–19.8, respectively. A recent review compared various MMMs having different types of fillers such as zeolites, silicas, carbon molecular sieves for O_2/N_2 separation, and reported that O_2/N_2 selectivities and O_2 permeabilities of these MMMs vary between 1–2.7×10^3 Barrers and 1–8, respectively [57]. That means many MOF/polymer MMMs that we

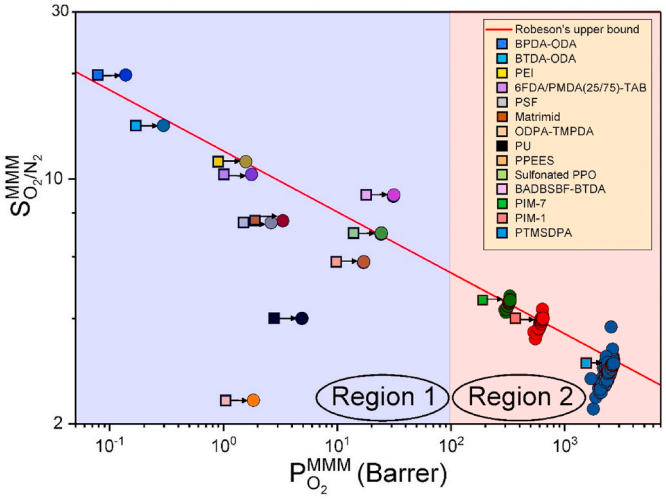


Fig. 4. Predicted O_2/N_2 selectivities and O_2 permeabilities of 78,806 MOF-based MMMs composed of 5629 MOFs and 14 polymers at 1 bar, 298 K. Squares (circles) represent pure polymers (MOF-based MMMs).

examined in this work can outperform traditional MMMs due to their high O_2/N_2 selectivity and O_2 permeability. We can divide Fig. 4 mainly into two regions to discuss the effect of MOF fillers on the performance of pure polymers regarding O_2/N_2 selectivities and O_2 permeabilities. The first region shows that the addition of MOFs into polymers having low O_2 permeabilities (≤100 Barrer) can improve permeabilities of pure polymers without altering O_2/N_2 selectivities. Incorporation of MOFs into PSF can increase O_2 permeability of pure PSF from 1.5 to 2.6 Barrers whereas O_2 selectivities of all MOF/PSF MMMs are almost the same as that of pure PSF (7.5). This suggests that the identity of MOFs is not important for changing the selectivity of polymers BTDA-ODA, 6FDA/PMDA (25/75)-TAB, PSF, Matrimid, PU, PPEES, ODPA-TMPDA. However, if a polymer is close to the upper bound in this region, such as PEI, BPDA-ODA, sulfonated PPO, MOFs can carry them above the upper bound. For example, O_2 permeability of sulfonated PPO increases upon the incorporation of MOFs from 14 to 24.5 Barrers and all MOF/sulfonated PPO MMMs can surpass the upper bound. Since BADBSBF-BTDA is already located well above the upper bound, using MOFs as fillers in this polymer enhances only O_2 permeability of pure polymer without changing its selectivity.

The second region of Fig. 4 shows that using of MOFs as fillers into MMMs considerably enhances the separation performance of polymers having high O_2 permeabilities (>100 Barrer). For polymers PIM-1, PIM-7, PTMSDPA, the identity of MOF is important. For example, incorporation of a highly O_2 permeable (4.1×10^4 Barrer) and selective (22.2) MOF such as PAJSAX into PTMSDPA increases both O_2 permeability (from 1.5×10^3 to 2.6×10^3 Barrers) and selectivity of pure polymer (from 2.98 to 3.78) which carries this MMM well above the upper bound. On the other hand, a MOF which has moderate O_2 permeability (1.5×10^4 Barrer) and O_2 selectivity (2.12) such as ACIBIY only enhances O_2 permeability of pure polymer (from 1.5×10^3 to 2.4×10^3 Barrer) without any change in O_2 selectivity (2.87). Results showed that incorporation of a MOF having moderate O_2 permeability (6.7×10^3 Barrer) but low selectivity (0.57) such as TIVXOM even decreases selectivity of polymer (from 2.98 to 2.46) with a slight increase in O_2 permeability (from 1.5×10^3 to 2.1×10^3 Barrers). Different than MOFs, enhancement in O_2 selectivity and reduction in O_2 permeability were reported for zeolite-incorporated PTMSP (polytrimethylsilylpropyne) membranes [58]. Therefore, proper selection of polymer and filler is crucial to obtain MMMs with high permeability and selectivity.

Our results so far presented that O_2 permeabilities of polymers are

significantly enhanced when MOF fillers are incorporated into different polymers but O_2 selectivities of polymers are not notably improved. When MOFs were incorporated into PPEES, the polymer having the lowest O_2/N_2 selectivity (2.33) among the ones we studied, the maximum achievable O_2 selectivity of MOF/PPEES MMM was calculated as 2.34, almost the same with selectivity of the polymer. Only for MMMs composed of highly permeable polymers such as PIM-1, PIM-7 and PTMSDPA, a slight increase was observed in O_2/N_2 selectivities. For example, incorporation of MOFs as fillers into PIM-1 enhances the selectivity of PIM-1 from 4.0 to 4.24. Many MOFs are not able to significantly improve O_2/N_2 selectivity of pure polymers, and to examine this, we studied how selectivity of pure MOFs and polymers affect the overall selectivity of MMMs.

The x axis of Fig. 5 shows the ratio of selectivity of a MOF membrane to that of a polymer membrane ($S^{MOF}_{O_2/N_2}/S^{P}_{O_2/N_2}$) and each line represents the ratio of O_2 permeability of a MOF membrane to that of a polymer ($P^{MOF}_{O_2}/P^{P}_{O_2}$) at fixed values. Here, we selected PIM-1 as the reference polymer since (i) it has been widely used for O_2/N_2 separation in experimental studies, (ii) incorporation of MOFs into PIM-1 led to MMMs that can surpass the upper bound as we discussed above. If O_2 selectivity of the MOF is less than that of PIM-1 (4), then the O_2 selectivity of the MMM cannot be higher than the selectivity of PIM-1 regardless of the permeability ratio. However, if the MOF has a higher selectivity than that of PIM-1 ($S^{MOF}_{O_2/N_2}/S^{P}_{O_2/N_2}>1$), the effect of MOF incorporation on the O_2/N_2 selectivity of MMM is more pronounced. If $S^{MOF}_{O_2/N_2}/S^{P}_{O_2/N_2}=10$ and $P^{MOF}_{O_2}/P^{P}_{O_2}=10$, O_2 selectivity of the MOF/PIM-1 MMMs can reach to 6.22. Another interesting result is that incorporation of MOFs having extremely high $P^{MOF}_{O_2}/P^{P}_{O_2}$ values ($>10^3$) does not change the selectivity of PIM-1 compared to the incorporation of MOFs having moderate $P^{MOF}_{O_2}/P^{P}_{O_2}$ values (10). Recent studies also showed that when the gas permeability of a polymer is extremely lower than that of pure MOF, the maximum achievable gas permeability of MMM computed by the Maxwell model is almost double of the permeability of pure polymer [13,59]. Our results showed that for O_2/N_2 separation, combining a polymer such as PIM-1 with a MOF having at least 10 times higher permeability and 100 times higher selectivity than PIM-1 ensures to obtain the best performing MMM.

Another important outcome of Fig. 5 is the identification of upper performance limits for MOF/polymer MMMs composed of 5629 MOFs and PIM-1 studied at two different simulation conditions. As shown by the colored region in Fig. 5, while $S^{MOF}_{O_2/N_2}/S^{P}_{O_2/N_2}$ was found to be in the range of 2.7×10^{-3} and 0.92 at infinite dilution, it was computed to be between 3.4×10^{-2} and 5.6 at the single-component gas condition. The larger range of $S^{MOF}_{O_2/N_2}/S^{P}_{O_2/N_2}$ obtained from the simulations performed at 1 bar led to higher selectivities for MOF/PIM-1 MMMs. In other words, if molecular simulations were performed at infinite dilution to compute the O_2 and N_2 permeabilities of MOF fillers, the maximum achievable selectivity of MOF/PIM-1 MMMs would be the same with O_2/N_2 selectivity of PIM-1 (4) regardless of $P^{MOF}_{O_2}/P^{P}_{O_2}$ values. However, if the single-component gas simulations were used and $P^{MOF}_{O_2}/P^{P}_{O_2}=10$, the maximum achievable selectivity of MMMs would be 5.35. Overall, Fig. 5 highlights that results obtained from molecular simulations of MOFs at infinite dilution underestimate O_2/N_2 selectivities of MMMs. Therefore, proper selection of a MOF having $P^{MOF}_{O_2}/P^{P}_{O_2}=1$ or 10 and at least $S^{MOF}_{O_2/N_2}/S^{P}_{O_2/N_2}=1$ under single-component gas condition can be a useful strategy to enhance O_2/N_2 selectivity and O_2 permeability of PIM-1.

3.3. Binary and ternary mixture separations

Experimental studies on polymer membranes for O_2/N_2 separation have been generally carried out using single-component gas measurement techniques. However, the current membrane technology aims to produce pure O_2 having a purity range of 25%–40% using the ambient air [60]. We note that to meet the industrial membrane-based O_2/N_2 separation, the purity of O_2 should be over 90% [57]. Therefore, mimicking the industrial air mixture in molecular simulation studies is necessary to understand the impact of purity of air mixture on the gas separation performances of MOF-based MMMs. Here, we focused on the top 10 MOF fillers (listed in Table S5) that lead to MOF/PIM-1 MMMs having the highest O_2/N_2 selectivities. We note that these MOFs have the highest O_2/N_2 membrane selectivities as pure membranes as shown in Fig. 2. We computed adsorption and diffusion properties of the best 10

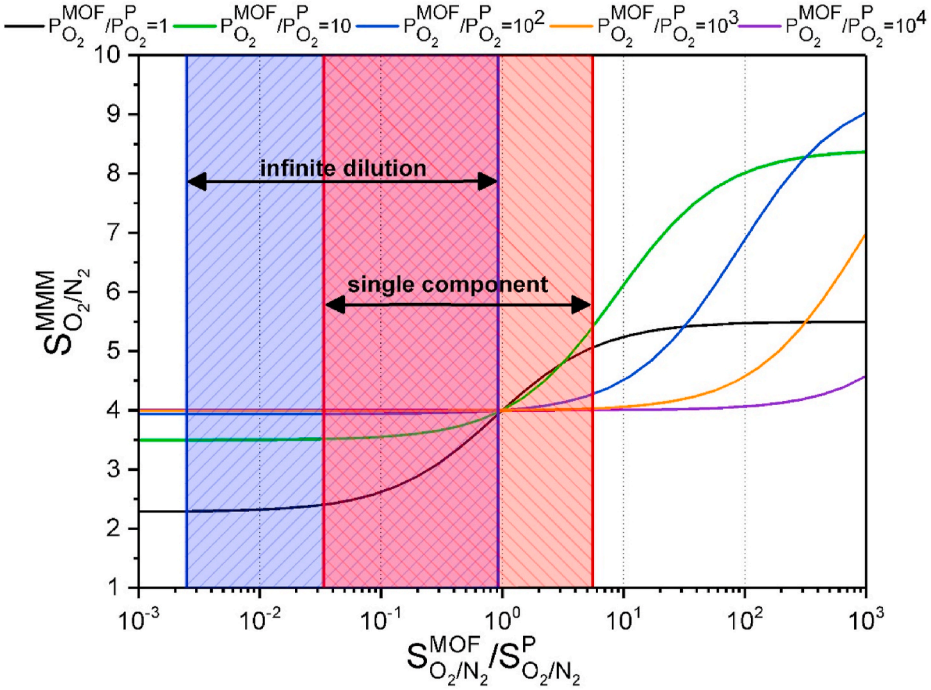


Fig. 5. Relations between selectivity of MMMs, MOFs, and polymers as a function of gas permeabilities. The polymer is PIM-1 with a selectivity of 4 [44].

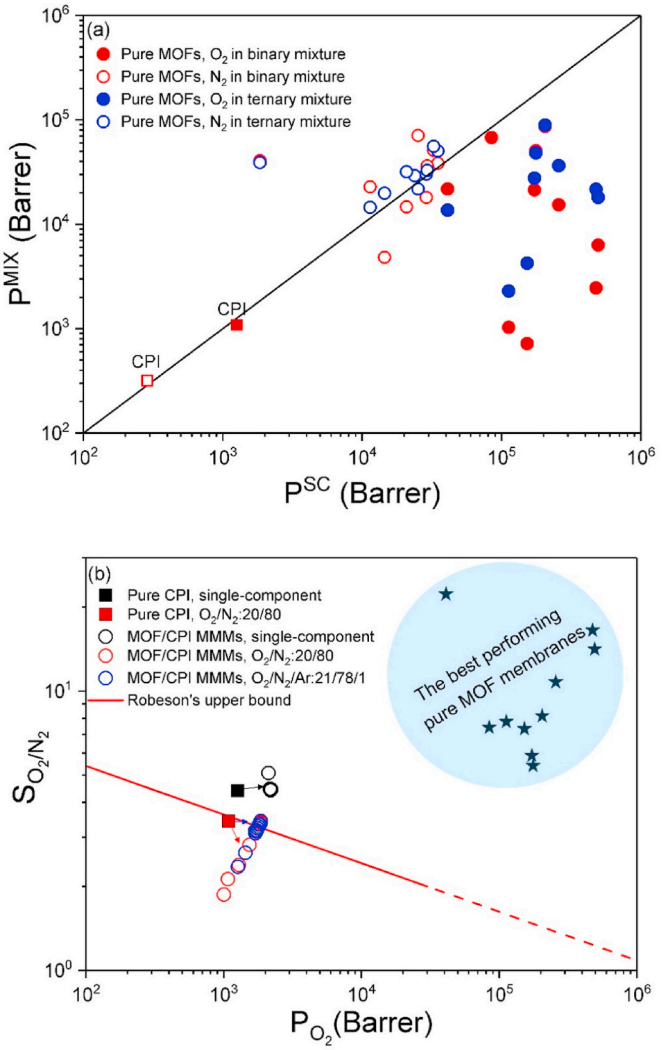


Fig. 6. (a) Predicted gas permeabilities of the top 10 MOFs and experimentally measured gas permeabilities of CPI polymer [61] at single-component gas and mixture conditions at 1 bar, 298 K. (b) Separation performances of MOF/CPI MMMs composed of the top 10 MOFs at single-component gas (black), binary mixture (red) and ternary mixture (blue) conditions. Stars represent O_2 permeabilities and O_2/N_2 selectivities of the top 10 MOFs computed at single-component gas condition. (For interpretation of the references to color in this figure legend, the reader is referred to the Web version of this article.)

MOFs by performing O_2/N_2:20/80 and O_2/N_2/Ar:20.98/77.92/1.1 mixture simulations at 1 bar, 298 K. Carbonized Polyimide (CPI) was studied as polymer since we were able to find its experimentally reported binary mixture permeability data for O_2/N_2 separation [61]. Fig. 6a compares mixture permeabilities of the top 10 MOFs and pure CPI with their single-component gas permeabilities. In mixture simulations, the bulk composition of N_2 is four times higher than that of O_2 and N_2 is preferentially adsorbed in MOFs. Calculated average N_2 diffusivities within these MOFs calculated from single-component gas simulations were found to be generally lower than those in binary and ternary mixtures simulations. As a result, N_2 permeabilities of MOFs in mixture simulations were generally higher than those calculated from single-component gas simulations. On the other hand, O_2 permeabilities of the top 10 MOFs were found to be lower in mixture simulations than those estimated from single-component gas simulations because of the smaller molar ratio of O_2. Similar results were also reported for the experimental gas permeability measurements of CPI polymer [61]. N_2 (O_2) permeability of CPI in the binary mixture was higher (lower) than its pure gas permeability. We note that due to the negligible amount of adsorbed Ar in the ternary mixture, N_2 and O_2 permeabilities obtained from binary and ternary mixture simulations were found to be similar. Fig. 6b compares single-component O_2/N_2 selectivities and O_2 permeabilities of MMMs composed of these MOFs (stars) and CPI (closed squares) with those obtained from mixture simulations. Since CPI does not have any experimentally reported ternary mixture permeability data in the literature, we used its binary mixture data [61] to predict O_2/N_2/Ar mixture separation performances of MMMs. Results showed that O_2 permeabilities and O_2/N_2 selectivities of MOF/CPI MMMs obtained from mixture simulations are much lower than those obtained from single-component gas simulations. We can conclude that gas permeabilities of MOFs acquired from single-component gas simulations provide a more optimistic judgement on the O_2/N_2 separation performance of MOF/CPI MMMs.

3.4. Flexible simulations

We predicted gas separation performances of MOFs by molecular simulations using rigid framework assumption, which has been used almost in all high-throughput computational screening studies since considering structural flexibility of MOFs enormously increases the computational time due to the addition of intramolecular interactions in the potential energy [9,11,12,59]. Moreover, defining an accurate force field for every single flexible MOF to consider bonded terms is challenging. We recently showed that structural flexibility of MOFs for CO_2/CH_4 and CH_4/H_2 separations may significantly affect gas separation performances of MOF membranes with narrow pore apertures as nearly the size of adsorbates [13,62,63]. For this reason, we performed computationally challenging flexible MD simulations for TUBJAD and XADCEM, representing a narrow-pored (~4 Å) MOF and a large-pored (~8 Å) MOF, respectively. TUBJAD was among the top 10 MOFs having the highest O_2/N_2 membrane selectivity at 1 bar, 298 K based on both pure MOF membrane and MMM calculations. XADCEM was selected considering the ranking of MOF-based PIM-1 membranes based on their O_2/N_2 selectivities. For the MMM calculations, we used CPI due to its experimentally available mixture gas permeation data.

Fig. 7 shows the single-component and mixture O_2 permeabilities and O_2/N_2 selectivities obtained from rigid and flexible MD simulations for MOF/CPI MMMs. The effect of structural flexibility of MOFs on O_2/N_2 selectivities and O_2 permeabilities of MOF/CPI MMM does not significantly vary depending on the pore sizes of MOFs. When flexibility was considered in simulations, single-component gas permeabilities and selectivities of both XADCEM/CPI and TUBJAD/CPI MMMs slightly reduced and retained their positions above the upper bound. Similarly, permeabilities of MOF/CPI MMMs decreased in both binary and ternary mixtures compared to those obtained from rigid MD simulations. The decrease in gas permeabilities of MOF/CPI MMMs in flexible simulations can be validated by the change in pore sizes of MOFs during MD simulations as shown in Fig. S5. Since the PLDs of XADCEM and TUBJAD decreased from 8.1 Å to 6.6 Å and from 4.35 Å to 3.54 Å, respectively, both gas diffusivities in these MOFs decreased, resulting in lower gas permeabilities. Results suggest that structural flexibility has a more pronounced effect on the calculated separation performance of narrow-pored MOFs rather than large-pored MOFs, especially for mixture separations. However, since the polymer phase dominates the Maxwell model and determines the performance of the MMM as we discussed in detail above, the contribution of MOF's flexibility to the permeability of MMMs is negligible both for narrow- and large-pored MOFs. Overall, we conclude that performing large-scale simulations of MOFs with a rigid framework assumption produces the required data to accurately identify the performance limits of MOF/polymer MMMs for O_2/N_2 separation.

4. Conclusion

In this study, we computationally explored O_2/N_2 separation

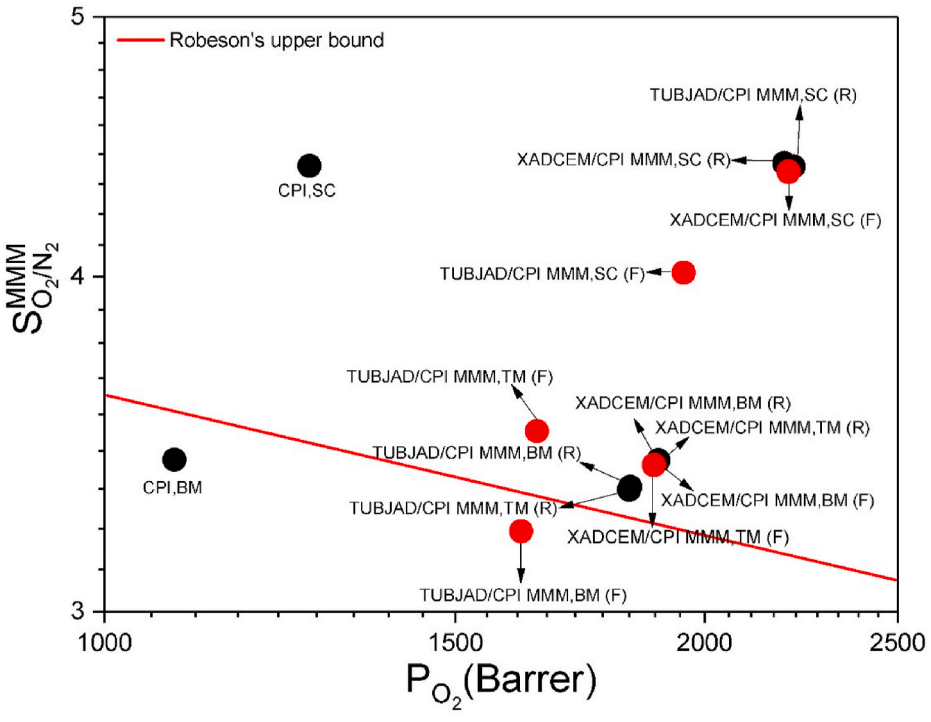


Fig. 7. Comparison of O_2 permeabilities and O_2/N_2 selectivities of MOF/CPI MMMs computed from rigid (R) and flexible (F) simulations at single-component gas (SC), binary mixture (BM), and ternary mixture (TM) conditions at 1 bar, 298 K. Black points represent the results obtained from rigid simulations and red points represent the results obtained from flexible simulations. (For interpretation of the references to color in this figure legend, the reader is referred to the Web version of this article.)

performance limits of 5629 pure MOF membranes and 78,806 MOF/polymer MMMs at infinite dilution and single-component gas conditions. We reported the highest value of O_2/N_2 selectivity and O_2 permeability of pure MOF membranes as 22.2 and 4×10^6 Barrer, respectively. The pure MOF membrane with the highest O_2/N_2 selectivity (22.2) was computed to have an O_2 permeability of 4.1×10^4 Barrer and the MOF with the highest O_2 permeability (4×10^6 Barrer) had an O_2/N_2 selectivity of 0.83. A high number of MOF membranes surpassed the upper bound, showing their great potentials to replace traditional polymer membranes in large-scale O_2/N_2 separations. Considering the challenges in fabricating defect-free membranes from nanoporous materials, we also examined MOFs as fillers in polymers to form MOF/polymer MMMs. We calculated the upper limits of O_2 permeabilities and O_2/N_2 selectivities of MOF/polymer MMMs as 2710.8 Barrer and 19.8 at 1 bar, 298 K. The MOF/polymer MMMs with the highest O_2/N_2 selectivity (19.8) was calculated to have an O_2 permeability of 0.14 Barrer and the MOF/polymer MMMs with the highest O_2 permeability (2710.8 Barrer) had an O_2/N_2 selectivity of 2.97. These results reveal that MOF/polymer MMMs outperform O_2/N_2 separation performances of polymer membranes and zeolite-based and carbon molecular sieves-based membranes. Considering easy processability and well-proven technology of making polymer membranes, MOF/polymer MMMs can be strong candidates for air separation. Results also showed that structural flexibility of MOFs does not significantly affect O_2 permeabilities and O_2/N_2 selectivities of MOF/CPI MMMs, suggesting that high-throughput screening of MOFs under rigid framework assumption will be a useful strategy to determine the top-performing MOF/polymer candidates. These results indicate that both MOF membranes and MOF/polymer MMMs can be used in air separation and guide the future studies to select the best combinations of MOFs and polymers for MMM applications.

CRediT author statement

Hilal Daglar: Methodology, Software, Validation, Investigation, Writing - Original Draft, Writing - Review & Editing.

Ilknur Erucar: Methodology, Software, Validation, Investigation, Writing - Original Draft, Writing - Review & Editing.

Seda Keskin: Conceptualization, Supervision, Methodology, Writing - Original Draft, Writing - Review & Editing.

Declaration of competing interest

The authors declare that they have no known competing financial interests or personal relationships that could have appeared to influence the work reported in this paper.

Acknowledgement

S.K. acknowledges ERC-2017-Starting Grant. This research has received funding from the European Research Council (ERC) under the European Union's Horizon 2020 research and innovation programme (ERC-2017-Starting Grant, grant agreement no. 756489-COSMOS).

Appendix A. Supplementary data

Supplementary data to this article can be found online at https://doi.org/10.1016/j.memsci.2020.118555.

References

[1] M. Eddaoudi, H. Li, O. Yaghi, Highly porous and stable Metal–Organic frameworks: structure design and sorption properties, J. Am. Chem. Soc. 122 (2000) 1391–1397.
[2] F.H. Allen, The Cambridge structural database: a quarter of a million crystal structures and rising, Acta Crystallogr. B 58 (2002) 380–388.
[3] Y.J. Colón, R.Q. Snurr, High-throughput computational screening of metal–organic frameworks, Chem. Soc. Rev. 43 (2014) 5735–5749.
[4] I. Erucar, S. Keskin, High-throughput molecular simulations of metal organic frameworks for CO_2 separation: opportunities and challenges, Front. Mater. 5 (2018) 4.
[5] J. Jiang, Computational screening of metal–organic frameworks for CO_2 separation, J. Appl. Polym. Sci 16 (2019) 57–64.
[6] A. Jain, R. Babarao, A.W. Thornton, Virtual screening of materials for carbon capture, Materials for Carbon Capture (2020) 117–151.
[7] P.G. Boyd, Y. Lee, B. Smit, Computational development of the nanoporous materials genome, Nat. Rev. Mater 2 (2017) 1–15.
[8] T. Watanabe, D.S. Sholl, Accelerating applications of metal–organic frameworks for gas adsorption and separation by computational screening of materials, Langmuir 28 (2012) 14114–14128.

[9] Z. Qiao, C. Peng, J. Zhou, J. Jiang, High-throughput computational screening of 137953 metal–organic frameworks for membrane separation of a $CO_2/N_2/CH_4$ mixture, J. Mater. Chem. A 4 (2016) 15904–15912.

[10] Z. Qiao, Q. Xu, J. Jiang, High-throughput computational screening of metal-organic framework membranes for upgrading of natural gas, J. Membr. Sci. 551 (2018) 47–54.

[11] C. Altintas, G. Avci, H. Daglar, A. Nemati Vesali Azar, S. Velioglu, I. Erucar, S. Keskin, Database for CO_2 separation performances of MOFs based on computational materials screening, ACS Appl. Mater. Interfaces 10 (2018) 17257–17268.

[12] H. Daglar, S. Keskin, Computational screening of metal–organic frameworks for membrane-based $CO_2/N_2/H_2O$ separations: best materials for flue gas separation, J. Phys. Chem. C 122 (2018) 17347–17357.

[13] C. Altintas, S. Keskin, Molecular simulations of MOF membranes and performance predictions of MOF/polymer mixed matrix membranes for CO_2/CH_4 separations, ACS Sustain. Chem. Eng. 7 (2019) 2739–2750.

[14] R. Stanger, T. Wall, R. Spörl, M. Paneru, S. Grathwohl, M. Weidmann, G. Scheffknecht, D. McDonald, K. Myöhänen, J. Ritvanen, Oxyfuel combustion for CO_2 capture in power plants, Int. J. Greenh. Gas Control. 40 (2015) 55–125.

[15] K. Adil, Y. Belmabkhout, R.S. Pillai, A. Cadiau, P.M. Bhatt, A.H. Assen, G. Maurin, M. Eddaoudi, Gas/vapour separation using ultra-microporous metal–organic frameworks: insights into the structure/separation relationship, Chem. Soc. Rev. 46 (2017) 3402–3430.

[16] P.Z. Moghadam, T. Islamoglu, S. Goswami, J. Exley, M. Fantham, C.F. Kaminski, R. Q. Snurr, O.K. Farha, D. Fairen-Jimenez, Computer-aided discovery of a metal–organic framework with superior oxygen uptake, Nat. Commun. 9 (2018) 1378.

[17] S. McIntyre, B. Shan, R. Wang, C. Zhong, J. Liu, B. Mu, Monte Carlo simulations to examine the role of pore structure on ambient air separation in metal-organic frameworks, Ind. Eng. Chem. Res. 57 (2018) 9240–9253.

[18] H. Demir, S.J. Stoneburner, W. Jeong, D. Ray, X. Zhang, O.K. Farha, C.J. Cramer, J. I. Siepmann, L. Gagliardi, Metal–organic frameworks with metal–catecholates for O_2/N_2 separation, J. Phys. Chem. C 123 (2019) 12935–12946.

[19] M.C. McCarthy, V. Varela-Guerrero, G.V. Barnett, H.-K. Jeong, Synthesis of zeolitic imidazolate framework films and membranes with controlled microstructures, Langmuir 26 (2010) 14636–14641.

[20] N. Hara, M. Yoshimune, H. Negishi, K. Haraya, S. Hara, T. Yamaguchi, Metal–organic framework membranes with layered structure prepared within the porous support, RSC Adv. 3 (2013) 14233–14236.

[21] Y. Zhang, Q. Gao, Z. Lin, T. Zhang, J. Xu, Y. Tan, W. Tian, L. Jiang, Constructing free standing metal organic framework MIL-53 membrane based on anodized aluminum oxide precursor, Sci. Rep. 4 (2014) 4947.

[22] A. Huang, H. Bux, F. Steinbach, J. Caro, Molecular-sieve membrane with hydrogen permselectivity: ZIF-22 in LTA topology prepared with 3-aminopropyltriethoxysilane as covalent linker, Angew. Chem. Int. Ed. 49 (2010) 4958–4961.

[23] A.F. Bushell, M.P. Attfield, C.R. Mason, P.M. Budd, Y. Yampolskii, L. Starannikova, A. Rebrov, F. Bazzarelli, P. Bernardo, J.C. Jansen, Gas permeation parameters of mixed matrix membranes based on the polymer of intrinsic microporosity PIM-1 and the zeolitic imidazolate framework ZIF-8, J. Membr. Sci. 427 (2013) 48–62.

[24] E.V. Perez, K.J. Balkus, J.P. Ferraris, I.H. Musselman, Mixed-matrix membranes containing MOF-5 for gas separations, J. Membr. Sci. 328 (2009) 165–173.

[25] M.J.C. Ordonez, K.J. Balkus Jr., J.P. Ferraris, I.H. Musselman, Molecular sieving realized with ZIF-8/Matrimid® mixed-matrix membranes, J. Membr. Sci. 361 (2010) 28–37.

[26] B. Zornoza, B. Seoane, J.M. Zamaro, C. Téllez, J. Coronas, Combination of MOFs and zeolites for mixed-matrix membranes, ChemPhysChem 12 (2011) 2781–2785.

[27] H.B.T. Jeazet, C. Staudt, C. Janiak, A method for increasing permeability in O_2/N_2 separation with mixed-matrix membranes made of water-stable MIL-101 and polysulfone, Chem. Commun. (J. Chem. Soc. Sect. D) 48 (2012) 2140–2142.

[28] L. Hao, K.-S. Liao, T.-S. Chung, Photo-oxidative PIM-1 based mixed matrix membranes with superior gas separation performance, J. Mater. Chem. 3 (2015) 17273–17281.

[29] P. Burmann, B. Zornoza, C. Téllez, J. Coronas, Mixed matrix membranes comprising MOFs and porous silicate fillers prepared via spin coating for gas separation, Chem. Eng. Sci. 107 (2014) 66–75.

[30] M.A. Rodrigues, J. de Souza Ribeiro, E. de Souza Costa, J.L. de Miranda, H. C. Ferraz, Nanostructured membranes containing UiO-66 (Zr) and MIL-101 (Cr) for O_2/N_2 and CO_2/N_2 separation, Separ. Purif. Technol. 192 (2018) 491–500.

[31] L. Xiang, D. Liu, H. Jin, L.-W. Xu, C. Wang, S. Xu, Y. Pan, Y. Li, Locking of phase transition in MOF ZIF-7: improved selectivity in mixed-matrix membranes for O_2/N_2 separation, Mater. Horiz. 7 (2020) 223–228.

[32] L.M. Robeson, The upper bound revisited, J. Membr. Sci. 320 (2008) 390–400.

[33] E. Gulcay, I. Erucar, Biocompatible MOFs for storage and separation of O_2: a molecular simulation study, Ind. Eng. Chem. Res. 58 (2019) 3225–3237.

[34] Y.G. Chung, E. Haldoupis, B.J. Bucior, M. Haranczyk, S. Lee, H. Zhang, K. D. Vogiatzis, M. Milisavljevic, S. Ling, J.S. Camp, Advances, updates, and analytics for the computation-ready, experimental metal–organic framework database: CoRE MOF 2019, J. Chem. Eng. 64 (2019) 5985–5998.

[35] T.F. Willems, C.H. Rycroft, M. Kazi, J.C. Meza, M. Haranczyk, Algorithms and tools for high-throughput geometry-based analysis of crystalline porous materials, Microporous Mesoporous Mater. 149 (2012) 134–141.

[36] K. Díaz, M. López-González, L.F. del Castillo, E. Riande, Effect of zeolitic imidazolate frameworks on the gas transport performance of ZIF8-poly (1, 4-phenylene ether-ether-sulfone) hybrid membranes, J. Membr. Sci. 383 (2011) 206–213.

[37] Y. Li, X. Wang, M. Ding, J. Xu, Effects of molecular structure on the permeability and permselectivity of aromatic polyimides, J. Appl. Polym. Sci. 61 (1996) 741–748.

[38] G. Maier, Gas separation with polymer membranes, Angew. Chem. Int. Ed. 37 (1998) 2960–2974.

[39] C.M. Zimmerman, W.J. Koros, Polypyrrolones for membrane gas separations. I. Structural Comparison of gas transport and sorption properties, J. Polym. Sci. B Polym. Phys. 37 (1999) 1235–1249.

[40] F. Hamad, T. Matsuura, Performance of gas separation membranes made from sulfonated brominated high molecular weight poly (2, 4-dimethyl-l, 6-phenyIene oxide), J. Membr. Sci. 253 (2005) 183–189.

[41] Y.-H. Kim, H.-S. Kim, S.-K. Kwon, Synthesis and characterization of highly soluble and oxygen permeable new polyimides based on twisted biphenyl dianhydride and spirobifluorene diamine, Macromolecules 38 (2005) 7950–7956.

[42] M. Teraguchi, T. Masuda, Poly (diphenylacetylene) membranes with high gas permeability and remarkable chiral memory, Macromolecules 35 (2002) 1149–1151.

[43] C. Duan, X. Jie, D. Liu, Y. Cao, Q. Yuan, Post-treatment effect on gas separation property of mixed matrix membranes containing metal organic frameworks, J. Membr. Sci. 466 (2014) 92–102.

[44] P.M. Budd, K.J. Msayib, C.E. Tattershall, B.S. Ghanem, K.J. Reynolds, N. B. McKeown, D. Fritsch, Gas separation membranes from polymers of intrinsic microporosity, J. Membr. Sci. 251 (2005) 263–269.

[45] D. Frenkel, B. Smit, Understanding molecular simulation: from algorithms to applications, Academic press, 2001.

[46] D. Dubbeldam, S. Calero, D.E. Ellis, R.Q. Snurr Raspa, Molecular simulation software for adsorption and diffusion in flexible nanoporous materials, Mol. Simulat. 42 (2016) 81–101.

[47] B.W. Dassault Systèmes Biovia, Release, BIOVIA Pipeline Pilot, Dassault Systèmes, San Diego, 2017.

[48] I. Erucar, S. Keskin, Unlocking the effect of H_2O on CO_2 separation performance of promising MOFs using atomically detailed simulations, Ind. Eng. Chem. Res. 59 (2020) 3141–3152.

[49] J.C. Maxwell, Electricity and magnetism, vol. 2, Dover, New York, 1954.

[50] I. Erucar, S. Keskin, Screening metal–organic framework-based mixed-matrix membranes for CO_2/CH_4 separations, Ind. Eng. Chem. Res. 50 (2011) 12606–12616.

[51] R. Krishna, Methodologies for evaluation of metal–organic frameworks in separation applications, RSC Adv. 5 (2015) 52269–52295.

[52] Z. Qiao, K. Zhang, J. Jiang, In silico screening of 4764 computation-ready, experimental metal–organic frameworks for CO_2 separation, J. Mater. Chem. A 4 (2016) 2105–2114.

[53] S.R. Venna, M.A. Carreon, Metal organic framework membranes for carbon dioxide separation, Chem. Eng. Sci. 124 (2015) 3–19.

[54] R.S. Murali, T. Sankarshana, S. Sridhar, Air separation by polymer-based membrane technology, Separ. Purif. Rev. 42 (2013) 130–186.

[55] E.V. Perez, K.J. Balkus Jr., J.P. Ferraris, I.H. Musselman, Mixed-matrix membranes containing MOF-5 for gas separations, J. Membr. Sci. 328 (2009) 165–173.

[56] Q. Song, S. Nataraj, M.V. Roussenova, J.C. Tan, D.J. Hughes, W. Li, P. Bourgoin, M. A. Alam, A.K. Cheetham, S.A. Al-Muhtaseb, Zeolitic imidazolate framework (ZIF-8) based polymer nanocomposite membranes for gas separation, Energy Environ. Sci. 5 (2012) 8359–8369.

[57] N.F. Himma, A.K. Wardani, N. Prasetya, P.T. Aryanti, I.G. Wenten, Recent progress and challenges in membrane-based O_2/N_2 separation, Rev. Chem. Eng. 35 (2019) 591–625.

[58] A. Fernández-Barquín, C. Casado-Coterillo, S. Valencia, A. Irabien, Mixed matrix membranes for O_2/N_2 separation: the influence of temperature, Membranes 6 (2016) 28.

[59] S. Budhathoki, O. Ajayi, J.A. Steckel, C.E. Wilmer, High-throughput computational prediction of the cost of carbon capture using mixed matrix membranes, Energy Environ. Sci. 12 (2019) 1255–1264.

[60] K. Chong, S. Lai, H. Thiam, H. Teoh, S. Heng, Recent progress of oxygen/nitrogen separation using membrane technology, J. Eng. Sci. Technol. 11 (2016) 1016–1030.

[61] N. Nishiyama, W. Momose, Y. Egashira, K. Ueyama, Partially carbonized Polyimide membranes with high permeability for air separation, J. Chem. Eng. Jpn. 36 (2003) 603–608.

[62] I. Erucar, S. Keskin, Computational modeling of bio-MOFs for CO_2/CH_4 separations, Chem. Eng. Sci. 130 (2015) 120–128.

[63] I. Erucar, S. Keskin, Computational assessment of MOF membranes for CH_4/H_2 separations, J. Membr. Sci. 514 (2016) 313–321.

[64] G. Avci, S. Velioglu, S. Keskin, High-throughput screening of MOF adsorbents and membranes for H_2 purification and CO_2 capture, ACS Appl. Mater. Interfaces 10 (39) (2018) 33693–33706.